Lipid Membrane Polarity Profiles by High-Field EPR

Dieter Kurad,* Gunnar Jeschke,† and Derek Marsh*
*Max-Planck-Institut für biophysikalische Chemie, Abteilung Spektroskopie, 37070 Göttingen, Germany; and †Max-Planck-Institut für Polymerforschung, Abteilung EPR-Spektroskopie, 55021 Mainz, Germany

ABSTRACT Profiles of polarity across biological membranes are essential determinants of the cellular permeability barrier and of the stability of transmembrane proteins. High-field electron paramagnetic resonance of systematically spin-labeled lipid chains is used here to determine the polarity profiles of cholesterol-containing phospholipid membranes. The polarity dependence of the g_{xx}-tensor element is opposite to the dependence on chain dynamics, and additionally has enhanced sensitivity to hydrogen bonding. Both features make high-field measurements superior to conventional determinations of local polarity from spin-label hyperfine couplings. The profile of g_{xx} in dimyristoyl phosphatidylcholine membranes with 5 or 40 mol% cholesterol is established with eleven positional isomers of phosphatidylcholine, spin labeled at positions $n = 4$–14 in the *sn*-2 chain. A sigmoidal barrier, centered about chain position $n_o \approx 8$, mirrors the corresponding sigmoidal trough obtained from the spin-label hyperfine coupling, A_{zz}. For the different positions, n, it is found that $\partial g_{xx}/\partial A_{zz} = -2.4\ T^{-1}$, a high value that is characteristic of hydrogen-bonded spin labels. This demonstrates that the transmembrane polarity profile registered by spin labels corresponds to water penetration into the membrane. Inhomogeneous broadening of the g_{xx}-spectral feature demonstrates heterogeneities of the water distribution in the regions of higher intramembrane polarity defined by $n < 8$. In the transition region between high- and low-polarity regions ($n \approx 8$), the g_{xx}-feature consists of two components characteristic of coexisting hydrated and nonhydrated states.

INTRODUCTION

The polarity profiles across lipid membranes are fundamental not only to the transport of water and polar solutes, and of oxygen and apolar solutes, but also to the energetics of insertion of proteins into membranes. Recently, we determined the polarity distribution across lipid membranes from measurements of the isotropic ^{14}N hyperfine splitting constants, a_o^N, of spin-labeled lipid chains at conventional electron paramagnetic resonance (EPR) frequencies (Marsh, 2001). In this work, a thermodynamic description was given of the troughlike transmembrane polarity profile. However, the direction of decreasing a_o^N is the same as that of the decreasing hyperfine anisotropy that arises from increasing rotational amplitude of the spin-labeled lipid chain segments (Hoffmann et al., 2000). The polarity dependence of the g_{xx}-element of the nitroxide g-tensor, on the other hand, is in the opposite direction to that of the hyperfine tensor and—most importantly—is opposite to that of increasing averaging of g_{xx} by both axial and off-axial rotation (see, e.g., Marsh et al., 2002). In principle, a far better discrimination between motional and polarity effects in spin-label spectra is therefore possible with high-field EPR. Even more importantly, essential information on the presence of H-bond donors (i.e., water molecules) is available from comparison of g-values with the ^{14}N hyperfine splittings (Kawamura et al., 1967; Steinhoff et al., 2000).

Here, we describe determination of the polarity profiles in lipid membranes containing cholesterol by measuring the g-tensors and hyperfine splittings of lipids that are spin labeled systematically at different positions down the fatty acid chain. High-field EPR is used to determine the g_{xx}-tensor element in frozen samples and to extract the isotropic g-value from anisotropic spectra of fluid membranes. Special attention is paid to the relative values of g-tensor and hyperfine shifts, which is diagnostic for water penetration into the membrane. In addition to establishing that the polarity profile is quite distinct from the mobility profile in fluid membranes, the high-field EPR measurements demonstrate that the transmembrane polarity profile is determined directly by water penetration, rather than by polarizing fields from the lipid polar groups. Further, the site selection offered by high-field spectroscopy specifically reveals the heterogeneity of water distribution in the hydrocarbon chain regions of the membrane and the coexistence of hydrated and nonhydrated states in the transition region of the troughlike polarity profile.

MATERIALS AND METHODS

Dimyristoyl phosphatidylcholine (DMPC) was obtained from Avanti Polar Lipids (Alabaster, AL) and cholesterol from Merck (Darmstadt, Germany). Oxazolidine-*N*-oxyl spin-labeled stearic acids (*n*-SASL) and the corresponding phosphatidylcholines spin labeled in the *sn*-2 chain (*n*-PCSL, 1-acyl-2-(*n*-(4,4-dimethyloxazolidine-*N*-oxyl)stearoyl)-*sn*-glycero-3-phosphocholine) were synthesized as described in Marsh and Watts (1982). DMPC, the required mole fraction of cholesterol, and 0.5–1 mol% *n*-PCSL spin label were codissolved in dichloromethane; the solvent was evaporated under a nitrogen gas stream; and the samples were dried under vacuum overnight. The dried lipid mixtures were then hydrated with an excess of buffer (100 mM KCl; 10 mM Tris; 1 mM EDTA) at pH 7.5. The resulting lipid dispersions were introduced into 0.5 or 0.2 mm inner diameter quartz capillaries, and then concentrated by centrifugation and the excess aqueous supernatant removed. The capillaries were flame sealed.

EPR spectra were recorded at a microwave frequency of 94 GHz on a Bruker (Karlsruhe, Germany) E680 heterodyne W-band EPR spectrometer with a TE_{011}-mode cylindrical cavity resonator and a split-coil superconducting magnet. The intermediate frequency of 9.6 GHz was provided by

Submitted March 11, 2003, and accepted for publication May 6, 2003.
Address reprint requests to Derek Marsh, E-mail: dmarsh@gwdg.de.

0006-3495/03/08/1025/09 $2.00

a Gunn diode oscillator, with upconversion by mixing with a phase-locked W-band Gunn source. Microwave power was normally 0.05 mW and loaded cavity Q was in the region of 1500 or higher, depending on the sample. Field scans with room temperature coils were of 30 mT width about a center magnetic field of 3.35 T. The magnetic field was calibrated with an Mn:CaO standard sample (Bruker, Karlsruhe). The Zeeman modulation frequency was 100 kHz, with peak-to-peak amplitude of 0.1 mT. Sampling times were typically 20 ms, with 1 K points and filter time constants of 5 ms. Spectra were signal-averaged over 1–16 scans, depending on signal strength. Measurements were made at variable temperature by using a thermostatted nitrogen gas-flow system. Peak maxima in the low- and high-field regions, and an intermediate region in the center of the spectrum (that is defined by powder-pattern simulations), were used to determine the effective g-tensor elements. No attempt was made to correct for any dispersion admixture in the experimental spectra. EPR spectra were recorded additionally at a microwave frequency of 9 GHz on a Varian Century Line spectrometer equipped with variable temperature facilities.

THEORETICAL BACKGROUND

The polarity dependence of the g-values for nitroxide spin labels has been analyzed by Kawamura et al. (1967). They used the theory of Stone (1963) for the g-tensor of π-radicals. The second-order perturbation expression for a particular diagonal element, g_{ii}, of the g-tensor involves cross terms between the magnetic field interaction and the spin-orbit coupling and is given by:

$$g_{ii} = g_e + 2\sum_{m\neq p}\frac{\sum_{k,k'}\langle\chi_p^{(k')}|l_i^{(k')}|\chi_m^{(k')}\rangle\zeta_k\langle\chi_m^{(k)}|l_i^{(k)}|\chi_p^{(k)}\rangle}{E_p - E_m}, \quad (1)$$

where p represents the unpaired electron orbital and m the other occupied and unoccupied orbitals. For nitroxide spin labels the unpaired electron is located in a $2p_z\pi$ orbital, and the other important orbitals are the bonding and antibonding σ-orbitals (b and a) of the N-O bond and the lone pair orbitals (n) on the oxygen. The superscripts k, k' refer to the atom centers N and O, and ζ_k is the corresponding spin-orbit coupling constant. For example, $\chi_m^{(k)}$ is the contribution of the atomic orbital from atom k to the molecular orbital m; the coefficient giving the weighting for this atomic orbital is designated $C_k^{(m)}$.

For a nitroxide spin label, the bonding and antibonding N-O σ-orbitals are composed of linear combinations of $2s$ and $2p_x$ orbitals. From Eq. 1 it therefore follows that the N-O σ-bond contributes only to the g_{yy}-element of the g-tensor. If the lone pair is confined to a $2p_y$ orbital on the oxygen, this then contributes only to the g_{xx}-element of the g-tensor. Under these circumstances the elements of the g-tensor are given by (Kawamura et al., 1967):

$$g_{xx} = g_e + \frac{2\zeta_O(C_{O,y}^{(n)})^2\rho_O}{E_p - E_n} \quad (2)$$

$$g_{yy} = g_e + 2\sum_{m}^{a,b}\frac{\zeta_N(C_{N,x}^{(m)})^2\rho_N + \zeta_O(C_{O,x}^{(m)})^2\rho_O + (\zeta_N + \zeta_O)C_{N,x}^{(m)}C_{O,x}^{(m)}p_{NO}}{E_p - E_m} \quad (3)$$

$$g_{zz} = g_e, \quad (4)$$

where g_e (=2.00232) is the free electron g-value; $C_{N,x}^{(b)}$, $C_{N,x}^{(a)}$ are coefficients of the nitrogen $2p_x$ orbital in the bonding and antibonding N-O σ-orbitals; $C_{O,y}^{(n)}$ is the coefficient of the oxygen $2p_y$ orbital in the lone pair orbital, etc. The unpaired electron densities on the nitrogen and oxygen atoms are ρ_N and ρ_O, respectively, and p_{NO} is the partial bond order of the unpaired electron orbital. If the lone pair orbital is an sp^2 hybrid, the above is modified only in that the lone pair then contributes also to the g_{yy} element, as well as to g_{xx}. A term similar to that in Eq. 2, but involving the $C_{O,x}^{(n)}$ admixture coefficient, is then added to the right-hand side of Eq. 3. Recent molecular orbital calculations, however, predict practically pure unhybridized $2p_y$-orbitals for the oxygen lone-pair electrons, i.e., $C_{O,y}^{(n)} \approx 1$ and $C_{O,x}^{(n)} \approx 0$ (Steinhoff et al., 2000). Because the lone pair lies closer in energy to the unpaired electron orbital than does the N-O σ-bonding orbital, it is expected that g_{xx} is the largest g-tensor element and also displays the greatest sensitivity to polarity.

The polarity dependence of the isotropic g-value, g_o, is therefore expected to be dominated by that of g_{xx}. The two are related by

$$g_{xx} = 3g_o - (g_{yy} + g_{zz}). \quad (5)$$

If the polarity dependence of g_{yy} and g_{zz} is small compared with that of g_{xx}, then g_o will be proportional to g_{xx} but with lower sensitivity to polarity. Data to be described later, for n-PCSL spin-labeled lipids in membranes of DMPC + 40 mol% cholesterol, yield a linear dependence of g_{xx} on g_o, but with a reduced gradient and intercept: $g_{xx} = (2.570 \pm 0.055)g_o - 3.145 \pm 0.0003$ ($R = 0.998$, $N = 11$). Both the reduced gradient and reduced intercept, relative to Eq. 5 with constant g_{yy} and g_{zz}, arise from the relatively small but nonvanishing polarity dependence of g_{yy}.

The polarity-induced shifts in g-tensor depend not only on the spin density, $\rho_O = 1-\rho_N$, on the oxygen atom but also on lowering of the lone-pair orbital energy, E_n (indicated by the blue shift in the n-π^* optical transition), as well as on delocalization of the lone-pair orbital (via the $C_{O,y}^{(n)}$ coefficient). Potentially, therefore, the polarity dependence of the g-tensor may considerably exceed that of the hyperfine tensor, which depends only on ρ_N, the unpaired spin density on the nitrogen (see later). Because the polarity dependence of the g-tensor is dominated by the oxygen lone-pair orbitals, it is expected that the g_{xx}-element will be particularly susceptible to hydrogen bonding. The polarity sensitivity of the g-values, relative to hyperfine splittings, is therefore greater in hydrogen-bonding solvents than in aprotic solvents (Kawamura et al., 1967; Owenius et al., 2001). Measurements of g-values at high fields therefore can distinguish water-accessible (i.e., hydrogen-bonding) environments from other polar environments (Steinhoff et al., 2000).

The polarity dependence of the isotropic hyperfine splitting constant, a_o^N, is related to the unpaired spin densities

on the nitrogen (ρ_N) and the oxygen (ρ_O) by a McConnell-type relation (Karplus and Fraenkel, 1961):

$$a_o^N = Q_N\rho_N + Q_{NO}\rho_O, \quad (6)$$

where the leading term is that involving Q_N ($\gg Q_{NO}$). The polarity dependence of the complete hyperfine tensor is determined by that of both the isotropic and anisotropic (i.e., dipolar) terms. For the diagonal z-element:

$$A_{zz} = a_o^N + 2|T_\perp^d|, \quad (7)$$

where $-|T_\perp^d|$ is the perpendicular element of the traceless hyperfine tensor that arises from the electron-nucleus dipolar interaction. Clearly, the latter depends directly on the unpaired spin density on the nitrogen: $T_\perp^d = T_{\perp,o}^d\rho_N$, where $T_{\perp,o}^d$ is the value of $T_\perp^d$ for $\rho_N = 1$. Combining Eqs. 6 and 7, the following linear relation is obtained between A_{zz} and the isotropic coupling constant, a_o^N:

$$A_{zz} = (1 + 2|T_{\perp,o}^d|/Q_N)a_o^N, \quad (8)$$

where the smaller term involving Q_{NO} in Eq. 6 has been neglected. Experimental data for oxazolidine-*N*-oxyl (DOXYL) nitroxides yields the following relationship (Marsh, 1981; Griffith et al., 1974):

$$A_{zz} = 2.35 \times a_o^N - 0.084\,\text{mT}, \quad (9)$$

where the smallness of the intercept justifies neglecting Q_{NO}. Taking a value of $|T_{\perp,o}^d| = (2/5)\,h^{-1}g_N\beta_N g\beta\langle r^{-3}\rangle = 47.8$ MHz for a ^{14}N 2p orbital (Whiffen, 1964), yields a value of $Q_N = 2.53$ mT. Using the full version of Eq. 6 leads to $Q_N = 2.59$ mT and $Q_{NO} = 0.06$ mT for an oxazolidine nitroxide. The latter value is considerably smaller than obtained previously for di-*tert*-butyl nitroxide (DTBN) and 2,2,6,6-tetramethylpiperidine-*N*-oxyl (TEMPO): $Q_N = 2.42 \pm 0.11$ mT and $Q_{NO} = 0.36 \pm 0.04$ mT (Cohen and Hoffman, 1973), and essentially justifies the approximation made in Eq. 8.

RESULTS

Frozen membranes

Fig. 1 (*left*) gives the HF-EPR spectra of the *n*-PCSL spin labels in frozen membranes of dimyristoyl phosphatidylcholine plus 40 mol% cholesterol at low temperature. All spectra are rigid powder patterns devoid of motional averaging. The polarity dependence is seen very clearly in the low-field g_{xx}-region of the spectra. An abrupt transition in position of the low-field peak takes place between 7-PCSL and 9-PCSL. That for the intermediate position, 8-PCSL, corresponds to a superposition of the two flanking positions. In addition, the widths of the low-field peak differ greatly between the two regions $n < 8$ and $n > 8$. Toward the center of the membrane the low-field peaks are remarkably narrow, whereas for positions close to the top of the chain they are much broader. This additional broadening, or g-strain, indicates a heterogeneity in polarity of the environment for the spin labels in the upper part of the chain (i.e., for $n < 8$). A likely origin is a statistical distribution of water molecules in this region of the membrane (see Theoretical Background section).

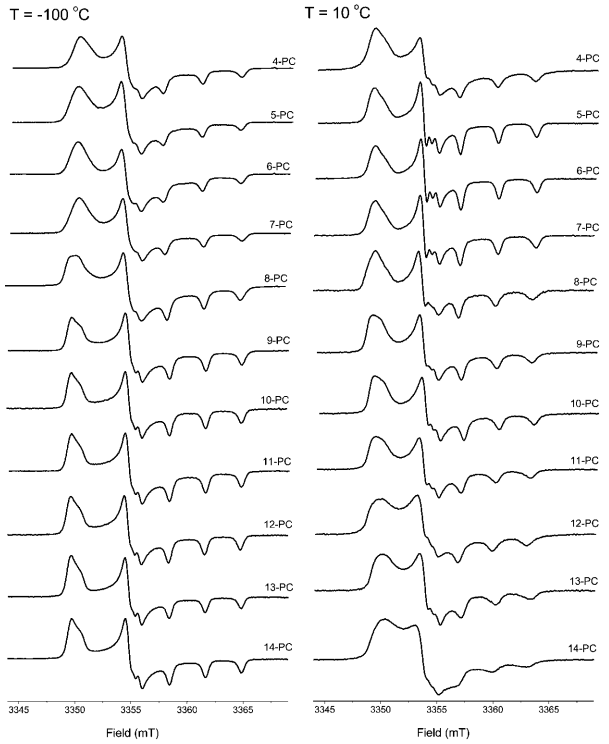

FIGURE 1 94 GHz EPR spectra of *n*-PCSL phosphatidylcholine spin-label positional isomers in membranes of dimyristoyl phosphatidylcholine + 40 mol% cholesterol at −100°C (*left*) and at +10°C (*right*).

The two-component nature of the spectrum from 8-PCSL, and the inhomogeneous broadening of the g_{xx}-peak, are illustrated in more detail in Fig. 2 by spectral subtraction. Spectrum *b* is the result of spectral titration by subtracting a single-component spectrum for $n > 8$ (viz., 14-PCSL) from the two-component spectrum of 8-PCSL. A suitable endpoint is reached that is very similar to a single-component spectrum for $n < 8$ (viz., 5-PCSL). Spectrum *d* is the result of the reverse spectral titration. Subtracting a single-component spectrum for $n < 8$ (viz., 6-PCSL) yields an endpoint that is very similar to a single-component spectrum for $n > 8$ (viz., 9-PCSL). The spectrum of 8-PCSL therefore corresponds to a mixture of spin labels in this transitional region, some of which are hydrogen bonded to water and some of which are not.

Fig. 2 shows that the lineshapes of the low-field, g_{xx}-feature differ greatly between $n < 8$ and $n > 8$. For the latter (see Fig. 2 *e*), the lines are relatively narrow and the A_{xx} ^{14}N-hyperfine splitting is partially resolved as a very pronounced shoulder on the high-field side of the g_{xx} peak. The half-width of an individual hyperfine line is ~0.5 mT as measured on the low-field manifold (see Fig. 2 *e*). For $n < 8$ (see Fig. 2 *a*), the additional inhomogeneous broadening of

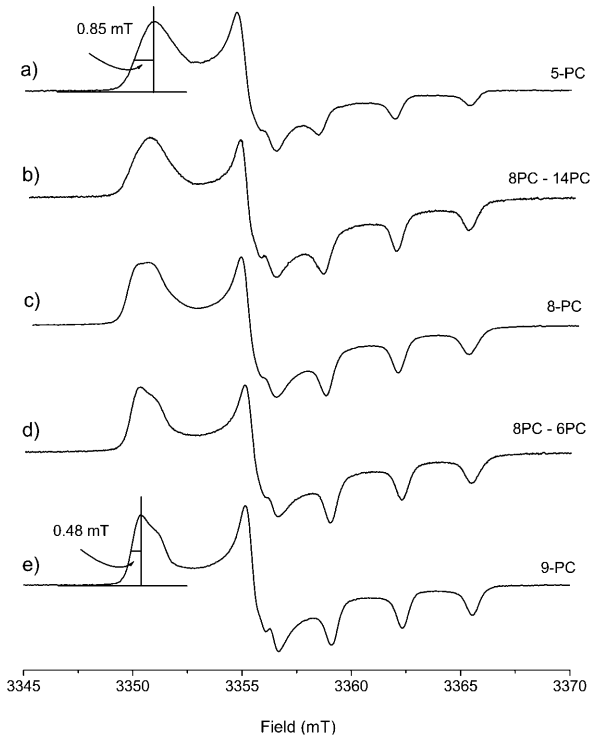

FIGURE 2 Resolution of the two components in the spectrum of 8-PCSL in DMPC/40 mol% cholesterol membranes at −100°C, by spectral subtraction. (*a*) Original spectrum of 5-PCSL. (*b*) Difference spectrum obtained by subtracting the spectrum of 14-PCSL from that of 8-PCSL, to yield a spectrum similar to *a*. (*c*) Original spectrum of 8-PCSL. (*d*) Difference spectrum obtained by subtracting the spectrum of 6-PCSL from that of 8-PCSL, to yield a spectrum similar to *e*. (*e*) Original spectrum of 9-PCSL.

the g_{xx}-feature exceeds the hyperfine splitting and a more symmetrical lineshape with a half-width of ~0.85 mT is obtained. The increase of linewidth in Fig. 2 *a*, relative to Fig. 2 *e*, represents the *g*-strain arising from heterogeneity in environmental polarity—most probably a heterogeneous distribution of water molecules—in those regions of the bilayer corresponding to upper parts of the lipid chains (i.e., $n < 8$).

Table 1 gives the *g*-tensors as a function of position of chain spin labeling, *n*, that are deduced from the spectra in the left panel of Fig. 1. Both g_{yy} and g_{zz} change very little with spin-label position, *n*, and g_{zz} is quite close to the free electron value of $g_e = 2.0023$, consistent with theoretical predictions (cf. Eqs. 3 and 4). The polarity dependence is reflected rather clearly in the values of the g_{xx}-element and of the hyperfine tensor element A_{zz}. Fig. 3 gives the transmembrane polarity profiles for one-half of the membrane as registered by these two parameters. The complementary nature of the polarity dependences of g_{xx} and A_{zz} are rather obvious in this plot. The troughlike form of the polarity profile is clearly discerned in Fig. 3 wherein larger *g*-values (and smaller hyperfine values) correspond to more hydrophobic environments.

TABLE 1 ***g*-Tensors (g_{xx}, g_{yy}, g_{zz}) and A_{zz} ^{14}N-hyperfine tensor element of *n*-PCSL spin labels in membranes of DMPC + 40 mol% cholesterol at −100°C**

n	g_{xx}	g_{yy}	g_{zz}	A_{zz} (mT)
4	2.00849	2.00573	2.00195	3.51
5	2.00857	2.00573	2.00195	3.47
6	2.00858	2.00579	2.00196	3.46
7	2.00859	2.00578	2.00197	3.45
8	2.00906	2.00578	2.00199	3.27
9	2.00916	2.00578	2.00202	3.23
10	2.00917	2.00578	2.00202	3.22
11	2.00918	2.00580	2.00202	3.22
12	2.00917	2.00578	2.00204	3.21
13	2.00918	2.00579	2.00204	3.20
14	2.00917	2.00578	2.00204	3.20

Corresponding data for membranes of DMPC + 5 mol% cholesterol at −100°C are given by the crosses in Fig. 3. It is seen immediately that there is little difference in the tensor elements of the low-cholesterol membranes from those with 40 mol% cholesterol. Unfortunately, even with admixture of 5 mol% cholesterol, residual spin-spin broadening prevents determination of accurate values for the $n = 8$ and $n = 10$ spin-label positional isomers.

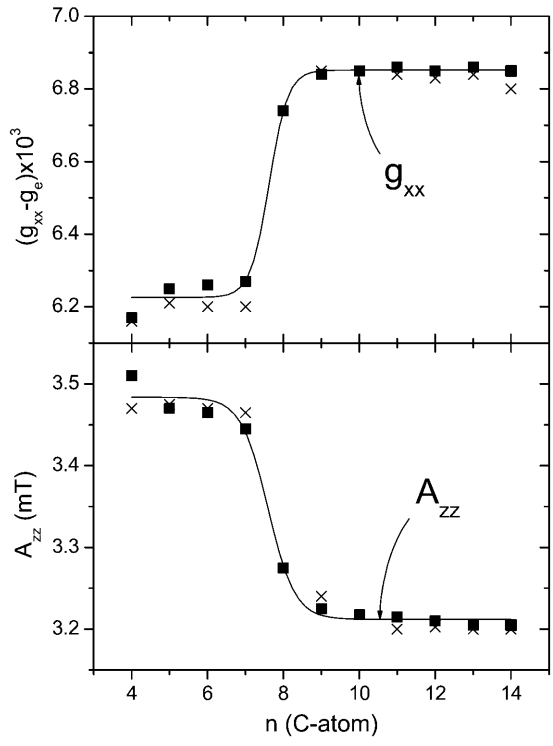

FIGURE 3 Dependence of g_{xx}-tensor element (*top*) and A_{zz} hyperfine tensor element (*bottom*) on spin-label chain position, *n*, in DMPC/40 mol% cholesterol membranes at −100°C (■). Lines represent nonlinear least squares fits to Eq. 10 and a corresponding equation for A_{zz}. The fitting parameters and uncertainties are given in Table 2. Data points for DMPC/5 mol% cholesterol are given by crosses.

Fluid membranes

The right panel of Fig. 1 gives HF-EPR spectra of the *n*-PCSL spin labels in liquid-ordered membranes of DMPC + 40 mol% cholesterol at +10°C. For spin labels close to the terminal methyl region of the chains, e.g., 14-PCSL, the *g*-value anisotropy is reduced and the lines are broadened considerably, relative to the rigid-limit spectra shown in the left panel. These spectral differences reflect the rotational dynamics of the lipid chains in the fluid state. The *g*-tensor elements are no longer determined solely by the local environmental polarity. Nevertheless, the *g*-value anisotropy is still reasonably well resolved at 10°C, and the trace of the partially averaged tensor elements: $g_o = \frac{1}{3}(\langle g_{xx}\rangle + \langle g_{yy}\rangle + \langle g_{zz}\rangle)$, can still be used as a polarity index.

Fig. 4 (*top*) gives the transmembrane polarity profile registered by g_o that is obtained from 94 GHz measurements at 10°C. For comparison, the bottom panel of Fig. 4 shows the polarity profile of the isotropic hyperfine coupling, a_o^N, that is determined from measurements at 9 GHz as previously described (Marsh, 2001). The values of g_o are not determined so precisely as those of g_{xx} from rigid-limit spectra. In addition, the polarity sensitivity of g_o is only one-third that of g_{xx} (see Eq. 5). Nonetheless, the *g*-value data clearly indicate a polarity profile in the fluid phase, which is complementary to that registered by the hyperfine coupling, a_o^N, just as do the measurements on frozen samples.

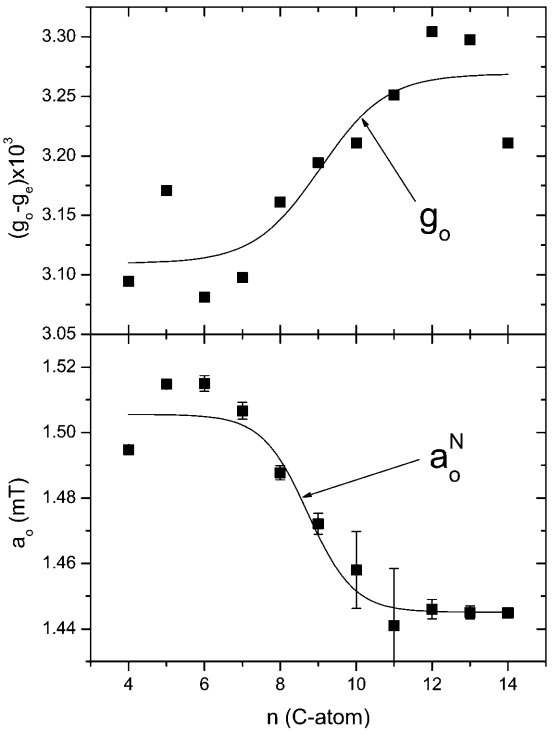

FIGURE 4 Dependence of the isotropic g_o-value (*top*) and isotropic ^{14}N-hyperfine coupling, a_o (*bottom*), on spin-label chain position, *n*, in DMPC/5 mol% cholesterol membranes in the fluid-ordered phase. a_o^N is obtained from 9 GHz measurements at $T > 25$°C, and g_o from the *g*-tensor trace at 10°C in 94 GHz measurements.

DISCUSSION

Here we establish the connection between the polarity profiles determined from high-field *g*-value measurements with those obtained previously from ^{14}N-hyperfine splittings. The high-field measurements are used to demonstrate the importance of water penetration in determining the transmembrane polarity profile. In particular, therefore, it will be seen that the inhomogeneous broadening arising from *g*-strain, and the coexisting spectral components in the transitional region (see Fig. 2), are to be attributed to lateral heterogeneities in the discrete distribution of water molecules at different depths in the hydrocarbon region of the membrane.

Polarity profiles

Frozen membranes

The dependence of the polarity profiles in Fig. 3 on spin-label position, *n*, are of the form introduced previously (Marsh, 2001):

$$g_{xx}(n) = \frac{g_{xx,1} - g_{xx,2}}{1 + e^{(n-n_{o,g})/\lambda_g}} + g_{xx,2}, \tag{10}$$

where $g_{xx,1}$ and $g_{xx,2}$ are the limiting values of g_{xx} at the polar headgroup and terminal methyl ends of the chain, respectively, $n_{o,g}$ is the value of *n* at the point of maximum gradient, corresponding to $g_{xx}(n_{o,g}) = (1/2)(g_{xx,1}+g_{xx,2})$, and λ_g is an exponential decay constant. Similar expressions apply to the isotropic *g*-value, g_o, and the corresponding ^{14}N hyperfine splitting constants A_{zz} and a_o^N. Table 2 gives the parameters that are obtained by fitting Eq. 10 to the spin Hamiltonian tensor elements measured at low temperature. Parameters are given for DMPC membranes containing both 40 and 5 mol% cholesterol. The low concentration (5 mol%)

TABLE 2 Parameters fitting the polarity profile of the g_{xx}-tensor elements and the A_{zz} hyperfine tensor element of *n*-PCSL spin labels in membranes of DMPC plus 40 or 5 mol% cholesterol at −100°C, according to Eq. 10

	DMPC/40 mol% chol	DMPC/5 mol% chol
$g_{xx,1}$	2.00855 ± 2.10^{-5}	2.00851 ± 1.10^{-5}
$g_{xx,2}$	2.00917 ± 1.10^{-5}	2.00915 ± 1.10^{-5}
$n_{o,g}$	7.63 ± 0.08	–*
λ_g	0.25 ± 0.05	–*
$A_{zz,1}$ (mT)	3.48 ± 0.01	3.472 ± 0.001
$A_{zz,2}$ (mT)	3.211 ± 0.006	3.201 ± 0.001
$n_{o,A}$	7.60 ± 0.09	–*
λ_A	0.36 ± 0.06	–*

*Residual spin-spin broadening in the spectra of 8-PCSL prevents precise definition of the parameters governing the transition region for DMPC/5 mol% cholesterol.

of cholesterol was used instead of DMPC alone in an attempt to minimize the rather drastic spin-spin broadening that is obtained in frozen samples for positions of spin labeling close to the middle of the chain (cf. Earle et al., 1994). Even so, data are missing for 8-PCSL, which precludes precise definition of the width and midpoint of the transition region for 5 mol% cholesterol. Essentially consistent values of n_o and λ are obtained from both the g_{xx} and A_{zz} profiles for DMPC/40 mol% cholesterol, as required if both are characterizing the same transmembrane polarity profile. None of the fitting parameters vary greatly over the range from –40°C to –130°C (data not shown). It is of interest to note that the g-shift, $\Delta g_{xx} = g_{xx,1} - g_{xx,2}$, between the outer and inner regions of the membrane is comparable in size to that calculated recently by density functional theory for hydrogen bonding of nitroxides to water (Owenius et al., 2001).

As is clear from Fig. 3, the transition from the low polarity interior to the high polarity exterior takes place at C-atom position $n_o \approx 8$ and is very sharp, being characterized by a small value of λ that corresponds to considerably less than a single CH_2 segment. This abrupt transition appears to be a feature of frozen membranes, because the polarity profiles in fluid membranes were found previously to be characterized by values of $\lambda \approx 1$ CH_2 unit (Marsh, 2001). Very similar values of the limiting spin Hamiltonian parameters $g_{xx,1}$, $g_{xx,2}$ and $A_{zz,1}$, $A_{zz,2}$ are obtained from membranes containing 5 and 40 mol% cholesterol. This contrasts with the situation found previously for fluid membranes with 0 and 50 mol% cholesterol (Marsh, 2001). Again this is most probably a consequence of freezing the membranes, which forces all water out of the hydrophobic core independent of the cholesterol content of the membrane. In the fluid state, however, there is measurable water penetration into the hydrophobic core of membranes not containing cholesterol. For membranes containing 50 mol% cholesterol, however, there is no water penetration at the center of the membrane in the fluid state (Marsh, 2001).

Comparison with the fluid phase is reinforced by the absolute values of the limiting parameters $A_{zz,1}$ and $A_{zz,2}$. Using Eq. 9 to convert the data from Table 2 into the corresponding effective isotropic hyperfine splitting constants yields values of $a^N_{o,1} = 1.51–1.52$ mT, $a^N_{o,2} = 1.40$ mT for frozen DMPC membranes with both 40 mol% and 5 mol% cholesterol. These values are close to those obtained for membranes of DMPC + 50 mol% cholesterol in the fluid phase, but differ substantially from membranes of DMPC alone in the fluid phase (Marsh, 2001). Most particularly, the value of $a^N_{o,2}$ corresponds to that found in mineral oil (Griffith et al., 1974), indicating that no water permeates the hydrophobic core in frozen DMPC membranes containing either 40 or 5 mol% cholesterol. Evidence for water penetration of the hydrophobic core for membranes containing 5 mol% cholesterol in the fluid phase is found from Fig. 4. The maximum value of $(g_{o,2} - g_e)$ is 3.30×10^{-3} at 10°C, as compared with $(g_{o,2} - g_e) = 3.35 \times 10^{-3}$ at −100°C (see Fig. 3 and Table 1). Correspondingly, the isotropic hyperfine splitting constant is $a^N_{o,2} = 1.445$ mT for DMPC + 5 mol% cholesterol at 10°C (Table 3).

Fluid membranes

Fig. 4 demonstrates that the isotropic g-value, g_o, reflects the profile of polarity across fluid lipid membranes in a way similar to that found for the isotropic hyperfine coupling, a^N_o (Marsh, 2001). The results from the g-values are significant because, unlike for hyperfine splittings, the influence of the polarity profile is opposite to that of the chain flexibility gradient in fluid membranes. However, it is found experimentally that measurements of a^N_o are more sensitive because all tensor elements are affected equally by polarity (cf. Eqs. 2–4 and 6–8). Table 3 gives the parameters that characterize the a^N_o-profiles by fitting with a sigmoidal form analogous to Eq. 10. Comparatively, the results obtained with DMPC plus 40 mol% cholesterol and 5 mol% cholesterol resemble those found previously for DMPC + 50 mol% cholesterol relative to DMPC without cholesterol (Marsh, 2001). The transition region of the profile is broader with fluid membranes than that found with frozen membranes. Also, there are characteristic differences in the limiting polarity parameters, $a^N_{o,1}$ and $a^N_{o,2}$, between fluid membranes with high and low cholesterol contents that are not found with frozen membranes.

Low-field EPR measurements demonstrate a pronounced dependence of the isotropic hyperfine splitting constant, a^N_o, on proton donor concentration in solvent mixtures (Gagua et al., 1978; Al-Bala'a and Bates, 1987). For fast exchange between hydrogen-bonded and nonhydrogen-bonded states that have isotropic hyperfine couplings, $a^N_{o,o}$ and $a^N_{o,h}$, respectively, the experimental value of a^N_o is given by the weighted average that is obtained by using the law of mass action:

$$a^N_o = \frac{a^N_{o,o} + a_{o,h}K_{A,h}[P]}{1 + K_{A,h}[P]}, \qquad (11)$$

where $K_{A,h}$ is the association constant for H-bond formation, which determines the relative population of the two species, and [P] is the proton donor concentration. An expression analogous to Eq. 11 holds also for the isotropic g-value, g_o, because g-shifts of the size induced by the H-bonding are directly proportional to the corresponding shifts in resonance line position.

TABLE 3 Parameters fitting the polarity profile of the hyperfine coupling, a^N_o, of *n*-PCSL spin labels in fluid membranes of DMPC plus 40 or 5 mol% cholesterol, according to Eq. 10

	DMPC/40 mol% chol	DMPC/5 mol% chol
$a^N_{o,1}$ (mT)	1.525 ± 0.006	1.506 ± 0.001
$a^N_{o,2}$ (mT)	1.433 ± 0.002	1.445 ± 0.001
$n_{o,a}$	9.10 ± 0.15	8.73 ± 0.11
λ_a	1.1 ± 0.2	0.6 ± 0.1

Equating the expression on the right hand of Eq. 11 with the corresponding expression from the version of Eq. 10 for a_o^N gives the proton donor (i.e., water) profile across the membrane:

$$K_{A,h}[P] = \frac{(a^N_{o,1} - a^N_{o,o}) + (a^N_{o,2} - a^N_{o,o})e^{(n-n_o)/\lambda}}{(a^N_{o,h} - a^N_{o,1}) + (a^N_{o,h} - a^N_{o,2})e^{(n-n_o)/\lambda}}. \quad (12)$$

This assumes that the polarity profile is dominated by the contribution from hydrogen bonding. If the concentration of proton donor in the center of the membrane is very low, then $a^N_{o,2} \approx a^N_{o,o}$ and Eq. 12 becomes:

$$K_{A,h}[P] \approx \frac{(a^N_{o,1} - a^N_{o,o})/(a^N_{o,h} - a^N_{o,o})}{(a^N_{o,h} - a^N_{o,1})/(a^N_{o,h} - a^N_{o,o}) + e^{(n-n_o)/\lambda}}. \quad (13)$$

If $a^N_{o,h} - a^N_{o,1} \gg a^N_{o,1} - a^N_{o,o}$, then the quotient in the denominator of Eq. 13 becomes equal to unity and the profile for [P] has the same form as Eq. 10. In fact, the concentration or activity [P] is expected to reflect a distribution of this form more directly than is the hyperfine splitting constant. Equation 10 represents a two-phase distribution between membrane regions $n > n_o$ and $n < n_o$, where the free energy of transfer, $(n - n_o)k_BT/\lambda$, increases linearly with distance from the $n = n_o$ plane. Equation 13 therefore provides some thermodynamic rationale as to why a^N_o, and correspondingly g_o, have a transmembrane profile described by Eq. 10.

Polarity and hydrogen bonding

In principle, the polarity profile registered by the spin Hamiltonian parameters of the spin-labeled lipids may have two different origins. One is the direct effect of hydrogen bonding by water molecules and the other is the polarizing field of neighboring polar molecular moieties (i.e., the effect of the local dielectric permittivity). As outlined in the Theoretical Background section, measurements of g-values by using high-field EPR preferentially favor the hydrogen-bonding component, i.e., water penetration into the membranes. Recent experimental and theoretical studies support this suggestion (Owenius et al., 2001). It was found that shifts in g_{xx} are much greater in hydrogen-bonding solvents than in aprotic solvents of comparable dielectric constant. Relative to toluene, the shifts in *n*-butanol ($\varepsilon = 17.8$) and ethanol ($\varepsilon = 24.3$) are $\Delta g_{xx} = -4.6 \times 10^{-4}$ and -3.9×10^{-4}, respectively, as compared with $\Delta g_{xx} = -0.4 \times 10^{-4}$ in acetone ($\varepsilon = 20.7$). In addition, shifts comparable to those in the protic solvents were predicted by quantum mechanical calculations using density functional theory: $\Delta g_{xx} = -4.4 \times 10^{-4}$ and -8.2×10^{-4} for hydrogen bonding to one and two water molecules, respectively (Owenius et al., 2001). In the two following subsections, comparisons of g-shifts with changes in hyperfine splittings are used to demonstrate that the polarity profiles established for lipid spin labels in membranes by high-field EPR are determined primarily by water penetration.

Frozen membranes

Fig. 5 shows the correlation of the g_{xx}-tensor element with the hyperfine tensor element A_{zz} for *n*-PCSLs ($n = 4$–9) in which the label is situated in the headgroup half of the phospholipid chain. Beyond this, i.e., for $n > 9$, both parameters have constant values in the hydrophobic core of the membrane. A reasonably linear correlation is found in Fig. 5, in agreement with results obtained in glassy solvents of differing polarities (Ondar et al., 1985; Owenius et al., 2001). The gradient in Fig. 5 is $\partial g_{xx}/\partial A_{zz} = -2.4 \pm 0.1\ T^{-1}$ ($R = -0.997$, $N = 6$), and a similar value is obtained for DMPC/5 mol% cholesterol at −100°C (data not shown). For a different nitroxide (pyrroline methanethiosulphonate), Steinhoff et al. (2000) have assigned a gradient of $-2.0 \pm 0.1\ T^{-1}$ to a protic (i.e., water-accessible) environment and of $-1.35 \pm 0.1\ T^{-1}$ to an aprotic environment, in bacteriorhodopsin. Corresponding values obtained recently in

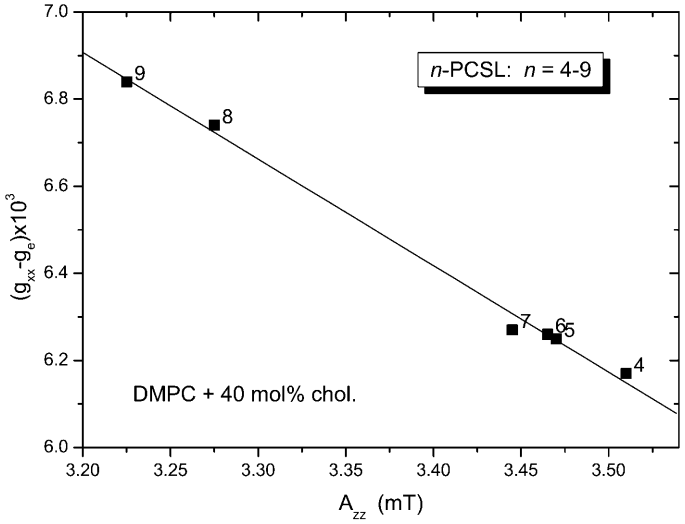

FIGURE 5 Correlation of the g_{xx}-tensor element with the ^{14}N hyperfine tensor element A_{zz} for *n*-PCSL spin labels in membranes of DMPC + 40 mol% cholesterol at −100°C. Data are given for the range $n = 4$–9.

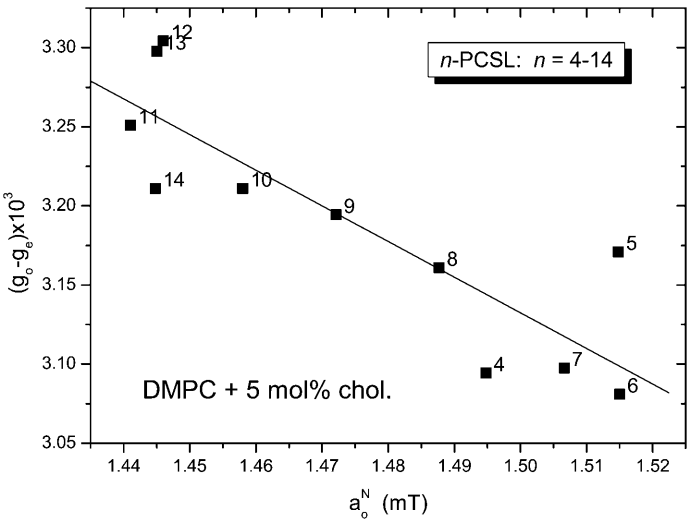

FIGURE 6 Correlation of the isotropic g-value, g_o, with the isotropic ^{14}N hyperfine coupling constant, a_o^N, for n-PCSL spin labels in membranes of DMPC + 5 mol% cholesterol in the fluid phase. a_o^N is obtained from 9 GHz measurements at $T > 25°C$, and g_o from the g-tensor trace at 10°C in 94 GHz measurements.

homogeneous solvents for the same spin label are: $-1.8\ T^{-1}$ and $\sim -0.8\ T^{-1}$ for protic and aprotic solvents, respectively (Owenius et al., 2001). The rather large slope obtained in Fig. 5 therefore suggests that water penetration into the membrane accounts for a large part of the polarity profile registered in Fig. 3.

Fluid membranes

The correlation between g_o and a_o^N in fluid membranes can be analyzed by use of Eq. 11 and its equivalent. For a dynamic equilibrium of hydrogen bonding, the following dependence of g_o on a_o^N is obtained:

$$g_o - g_e = \left(\frac{g_{o,h} - g_{o,o}}{a^N_{o,h} - a^N_{o,o}}\right) a_o^N + \frac{(g_{o,o} - g_e)a^N_{o,h} - (g_{o,h} - g_e)a^N_{o,o}}{a^N_{o,h} - a^N_{o,o}}, \tag{14}$$

where $g_{o,h}$ and $g_{o,o}$ are defined for the hydrogen-bonded and nonhydrogen-bonded states, as for $a^N_{o,h}$ and $a^N_{o,o}$ above. From low-field measurements in water and in hexane or toluene, the gradient is given approximately by: $(g_{o,h} - g_{o,o})/(a^N_{o,h} - a^N_{o,o}) \approx -2.4\ T^{-1}$ for both di-*tert*-butyl nitroxide (Griffith et al., 1974) and the pyrroline-*N*-oxy methanethiosulphonate (Owenius et al., 2001).

For measurements with n-PCSL in the fluid phase of DMPC/5 mol% cholesterol membranes (see Fig. 6): $\partial g_o/\partial a_o^N = -2.3 \pm 0.4\ T^{-1}$ and the intercept in Eq. 14 is 0.065 ± 0.006 ($R = -0.865$, $N = 11$). Again, the size of the gradient suggests that water penetration contributes strongly to the polarity profile registered by the isotropic spin Hamiltonian parameters in the fluid phase.

The above analysis confirms that the inhomogeneous broadening and two-component high-field spectra that are shown in Fig. 2 are to be attributed to the discrete nature of the water distribution in the hydrocarbon core, as opposed to any other type of membrane heterogeneity. This result both complements and augments recent electron spin echo modulation experiments with D_2O, which also give direct evidence for water penetration (Bartucci et al., 2003). It is of interest to consider what advantage can be gained by proceeding to yet higher fields and microwave operating frequencies than 94 GHz. An increase in inhomogeneous broadening from heterogeneous water distribution and an increased resolution of hydrated and dehydrated states are to be expected. In the fluid state, any residual slow-motional contributions will be driven into the rigid limit at higher frequencies, thus ensuring that isotropic tensor averages are determined rigorously from solely fast motions (cf. Livshits and Marsh, 2003).

CONCLUSIONS

High-field EPR of spin-labeled lipids contributes in three decisive ways to the determination of transmembrane polarity profiles. First, measurements of the g-values are able to distinguish diagnostically between profiles of decreasing polarity and of increasing chain flexibility. Second, the size of the shifts in g-value, relative to those in hyperfine splitting, demonstrates the contribution of H-bonding (i.e., water penetration) to the polarity profile. This then allows the spectroscopically determined profile to be defined thermodynamically in terms of water penetration. Third, the site selectivity at high field allows resolution of individual hydration/polarity states from splitting or inhomogeneous broadening of the g_{xx}-spectral peak (see Fig. 2). The discrete nature of these heterogeneities in polarity is attributable to individual water molecules.

We thank Frau B. Angerstein for synthesis of spin-labeled lipids and valuable technical assistance.

This work was supported by the Priority Programme ''High-Field EPR'' of the Deutsche Forschungsgemeinschaft.

REFERENCES

Al-Bala'a, I., and R. D. Bates Jr. 1987. Medium effects on ESR spectra in studies of hydrogen-bonded transient solvent-solute complexes. *J. Magn. Reson.* 73:78–89.

Bartucci, R., R. Guzzi, D. Marsh, and L. Sportelli. 2003. Intramembrane polarity by electron spin echo spectroscopy of labeled lipids. *Biophys. J.* 84:1025–1030.

Cohen, A. H., and B. M. Hoffman. 1973. Hyperfine interactions in perturbed nitroxides. *J. Am. Chem. Soc.* 95:2061–2062.

Earle, K. A., J. K. Moscicki, M. T. Ge, D. E. Budil, and J. H. Freed. 1994. 250-GHz electron spin resonance studies of polarity gradients along the aliphatic chains in phospholipid membranes. *Biophys. J.* 66:1213–1221.

Gagua, A. V., G. G. Malenkov, and V. P. Timofeev. 1978. Hydrogen-bond contribution to isotropic hyperfine splitting constant of a nitroxide free-radical. *Chem. Phys. Lett.* 56:470–473.

Griffith, O. H., P. J. Dehlinger, and S. P. Van. 1974. Shape of the hydrophobic barrier of phospholipid bilayers. Evidence for water penetration in biological membranes. *J. Membr. Biol.* 15:159–192.

Hoffmann, P., K. Sandhoff, and D. Marsh. 2000. Comparative dynamics and location of spin-labelled sphingomyelin and phosphatidylcholine in dimyristoyl phosphatidylcholine membranes studied by EPR spectroscopy. *Biochim. Biophys. Acta.* 1468:359–366.

Karplus, M., and G. K. Fraenkel. 1961. Theoretical interpretation of carbon-13 hyperfine interactions in electron spin resonance spectra. *J. Chem. Phys.* 35:1312–1323.

Kawamura, T., S. Matsunami, and T. Yonezawa. 1967. Solvent effects on the *g*-value of di-*t*-butyl nitric oxide. *Bull. Chem. Soc. Japan.* 40:1111–1115.

Livshits, V. A., and D. Marsh. 2003. Simulation of high-field EPR spectra from spin labels in membranes. *In* Very High Frequency (VHF) ESR/EPR, Biological Magnetic Resonance, Vol. 22. O. Y. Grinberg and L. J. Berliner, editors. Kluwer Academics, New York. In press.

Marsh, D. 1981. Electron spin resonance: spin labels. *In* Membrane Spectroscopy. Molecular Biology, Biochemistry and Biophysics, Vol. 31. E. Grell, editor. Springer-Verlag, Berlin, Heidelberg, New York. 51–142.

Marsh, D. 2001. Polarity and permeation profiles in lipid membranes. *Proc. Natl. Acad. Sci. USA.* 98:7777–7782.

Marsh, D., D. Kurad, and V. A. Livshits. 2002. High-field electron spin resonance of spin labels in membranes. *Chem. Phys. Lipids.* 116:93–114.

Marsh, D., and A. Watts. 1982. Spin-labeling and lipid-protein interactions in membranes. *In* Lipid-Protein Interactions, Vol. 2. P. C. Jost and O. H. Griffith, editors. Wiley-Interscience, New York. 53–126.

Ondar, M. A., O. Y. Grinberg, A. A. Dubinskii, and Y. S. Lebedev. 1985. Study of the effect of the medium on the magnetic-resonance parameters of nitroxyl radicals by high-resolution EPR spectroscopy. *Sov. J. Chem. Phys.* 3:781–792.

Owenius, R., M. Engström, M. Lindgren, and M. Huber. 2001. Influence of solvent polarity and hydrogen bonding on the EPR parameters of a nitroxide spin label studied by 9-GHz and 95-GHz EPR spectroscopy and DFT calculations. *J. Phys. Chem. A.* 105:10967–10977.

Steinhoff, H. J., A. Savitsky, C. Wegener, M. Pfeiffer, M. Plato, and K. Möbius. 2000. High-field EPR studies of the structure and conformational changes of site-directed spin labeled bacteriorhodopsin. *Biochim. Biophys. Acta.* 1457:253–262.

Stone, A. J. 1963. *g*-factors of aromatic free radicals. *Mol. Phys.* 6:509–515.

Whiffen, D. H. 1964. Information derived from anisotropic hyperfine couplings. *J. Chim. Phys.* 61:1589–1591.